Negative Refractive Index in Chiral Metamaterials

Shuang Zhang,[1] Yong-Shik Park,[1] Jensen Li,[1] Xinchao Lu,[2] Weili Zhang,[2] and Xiang Zhang[1,3,*]

[1]*Nanoscale Science and Engineering Center, University of California, 5130 Etcheverry Hall, Berkeley, California 94720-1740, USA*
[2]*School of Electrical and Computer Engineering, Oklahoma State University, Stillwater, Oklahoma 74078, USA*
[3]*Materials Sciences Division, Lawrence Berkeley National Laboratory, 1 Cyclotron Road Berkeley, California 94720, USA*

(Received 18 August 2008; revised manuscript received 16 December 2008; published 12 January 2009)

We experimentally demonstrate a chiral metamaterial exhibiting negative refractive index at terahertz frequencies. The presence of strong chirality in the terahertz metamaterial lifts the degeneracy for the two circularly polarized waves and allows for the achievement of negative refractive index without requiring simultaneously negative permittivity and negative permeability. The realization of terahertz chiral negative index metamaterials offers opportunities for investigation of their novel electromagnetic properties, such as negative refraction and negative reflection, as well as important terahertz device applications.

DOI: 10.1103/PhysRevLett.102.023901 PACS numbers: 42.25.Bs, 42.25.Ja, 78.20.Ci

Negative index metamaterials (NIMs) give rise to many unusual properties and phenomena, which may lead to important applications such as a superlens, subwavelength cavity and slow light devices [1–7]. The first negative index metamaterial was demonstrated in the microwave frequencies, which consisted of two functional subsets: the so called ''split ring resonators'' for negative magnetic response, and thin metallic wires for negative electric response [1]. Since the first demonstration, many variations of NIMs with different configurations and operating at different frequencies have been experimentally investigated; however, the basic mechanism of achieving a negative index through simultaneously negative permittivity ε and negative permeability μ still remains the same. Recently, an alternative route toward negative refraction by utilizing material chirality has been first theoretically proposed by Tretyakov [8], and later independently proposed by Pendry and Monzon [9,10], which may bring new perspectives and functionalities that go beyond the conventional NIMs [8,11,12].

A material is defined to be chiral if it lacks any planes of mirror symmetry. In terms of electromagnetic responses, chiral material is characterized by a cross coupling between the electric and the magnetic dipoles along the same direction. This results in the breaking of degeneracy between the two circularly polarized waves; i.e., the refractive index is increased for one circular polarization and reduced for the other. Given the chirality is strong enough, negative refraction may occur for one circularly polarized wave, while for the other circular polarization the refractive index remains positive. This gives rise to interesting phenomena that conventional NIMs do not exhibit, such as *negative reflection* for electromagnetic waves incident onto a mirror embedded in such a medium [13]. Furthermore, in the special case where two circularly polarized waves having refractive indices of the same amplitude but opposite signs, the light incident onto the mirror would be reflected back at exactly the same direction. This phenomenon of time reversal is similar to that of light reflected from a phase conjugate mirror, but without involving nonlinearity.

Terahertz is a unique frequency range with many important applications such as security detection and gas phase molecule sensing [14]. However, the devices for manipulating the terahertz wave are considerably limited. Consequently, the development of artificial materials with unusual optical properties at this frequency region is especially important. Recently, the development in metamaterial research has led to the achievement of unusual optical functionalities at terahertz frequencies [15–20]. However, due to the complexity of the chiral metamaterial geometry, experimental realizations of chiral NIMs at the terahertz and even higher frequencies still remain major challenges. Although chiral metamaterials were recently studied at the microwave, terahertz, and optical frequencies using a simplified bilayer configuration, but no evidence of negative refractive index has been shown in these works [21–24]. Here we experimentally demonstrate a negative index chiral metamaterial in terahertz. This would open doors to exploration of the interesting properties associated with chiral NIMs, as well as broad device applications at terahertz frequencies.

The chiral metamaterial design is based on a vertical metallic chiral resonator, in which the chirality is introduced by tilting the loop of the resonator out of the plane with its gap [Fig. 1(a)]. The chiral resonator is equivalent to a micro-sized inductor-capacitor (LC) resonant circuit, with the inductor formed by the loop and the capacitor formed between the two bottom metal strips [Fig. 1(b)]. Oscillating current flowing through the metal loop can be excited by either an electric field across the gap or a magnetic field perpendicular to the loop, which in turn generate strong electric and magnetic responses [25]. Therefore, this structure can be considered as the combi-

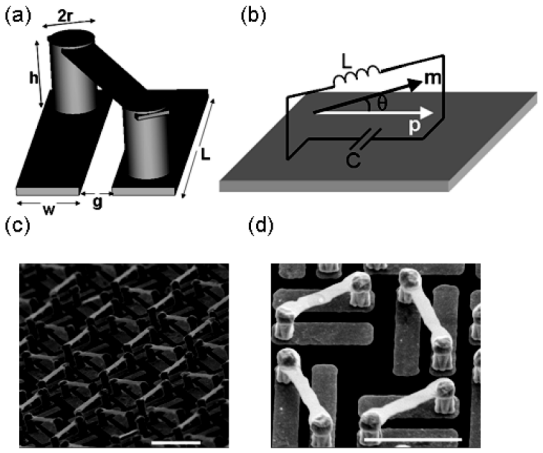

FIG. 1. (a) The schematic of the chiral structure made of gold, with the dimensions indicated in the figure: $L = 20\ \mu$m, $h = 4.5\ \mu$m, $r = 1.6\ \mu$m, $w = 4.4\ \mu$m, $g = 2.3\ \mu$m. The thicknesses of the bottom strips and the top bridge are 0.6 and 0.3 μm, respectively. The bottom strips make an angle $\theta = 29.25°$ with the top bridge. (b) The inductor-capacitor circuit model of the chiral structure, which functions effectively as an electric dipole (white arrow, along the direction of capacitor) and a magnetic dipole (dark arrow, along the direction of inductor) forming an angle θ. (c),(d) the SEM images of the chiral metamaterials at tilted angle. The size of the unit cell is 40 μm by 40 μm. The scale bars are 20 μm.

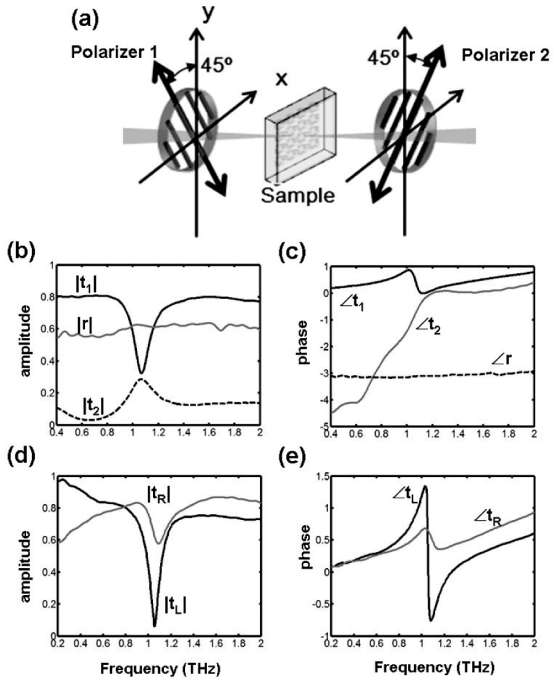

FIG. 2. Time-domain terahertz measurements of the chiral metamaterials. (a) Two-polarizer setup to measure the transmission coefficients. Terahertz wave propagates along $+z$ direction. The polarization of terahertz source and detection are in the horizontal direction (x axis). The polarizers are tilted 45° with respect to the vertical direction (y axis). Polarizer 2 is either parallel or perpendicular to polarizer 1, for the measurement of t_1 or t_2, respectively. (b) The amplitudes of t_1 (black solid) and t_2 (black dashed) and reflectance r (gray). (c) The phases of t_1 (black), t_2 (dashed), and r (gray). (d) The transmission amplitudes for left-handed (black) and right-handed (gray) circular polarizations. (e) The transmission phases for left-handed (black) and right-handed (gray) circular polarizations.

nation of an electric dipole and a magnetic dipole, as indicated in Fig. 1(b). Since the electric and magnetic dipoles share the same structural resonance, the excitation of one dipole would inevitably lead to the excitation of the other. Because of the fact that the angle between directions of the two dipoles is small, a strong chiral behavior is expected, which, with properly designed geometric parameters, will lead to negative refraction for circularly polarized waves.

We have fabricated large scale (1.5 cm by 1.5 cm) chiral negative index metamaterials. The SEM images of the structure are shown in Figs. 1(c) and 1(d). The chiral metamaterials is characterized by terahertz–time-domain spectroscopy (THz-TDS) [26,27]. The THz-TDS system has a usable bandwidth of 0.1–4.5 THz (3 mm-67 μm) and a signal to noise ratio (S/N) of >15 000:1 [28]. In the transmission measurement, the chiral sample was placed midway between the transmitter and receiver modules at the waist of terahertz beam [Fig. 2(a)]. Two free standing metal wire polarizers were employed, one in front of and one after the sample to measure the transmission of the same polarization state as that of the incident wave t_1 ($P1//P2$) and that of the perpendicular polarization state t_2 ($P1 \perp P2$). The THz-TDS is capable of measuring the temporal profiles of the electric fields $E_i(t)$ ($i = 1, 2$) of the picosecond terahertz pulse transmitting through the sample [26,29]. The complex coefficients for the transmissions can be obtained by taking the Fourier transform of the time signals, $\tilde{E}_i(\omega) = \mathcal{F}[E_i(t)]$, and calibrated over a bare silicon wafer identical to the substrate of the sample, i.e., $t_i(\omega) = \tilde{E}_i(\omega)/\tilde{E}_{Si}(\omega)$. The corresponding phase was obtained from the measured transmission through the relation, $\phi(t_i) = \arg(t_i)$. Owing to the fourfold rotational symmetry of the sample, the transmission properties do not rely on the orientation of the sample relative to the polarization of the incident wave, which was confirmed by additional transmission measurements with sample rotated by 90°. For left and right circularly polarized beams the transmission coefficients t_L and t_R can be inferred by

$$t_L = t_1 - it_2 \qquad t_R = t_1 + it_2. \tag{1}$$

The measured transmission amplitudes and phases for t_1 and t_2 are shown in Figs. 2(b) and 2(c). A resonance occurs around 1 THz, exhibiting a dip in t_1 and a peak in t_2, indicating a strong chiral behavior that leads to the conversion of a large portion of the energy to the other linear polarization. The resonance is accompanied by a steep slope in the relative phases of the transmissions [Fig. 2(c)]. In contrast to the transmission spectra, the reflectance of

the chiral metamaterials for terahertz wave does not show pronounced features. The reflectance amplitude is around 0.6 in the range of frequency from 0.2 to 2 THz, and the reflectance phase is close to $-\pi$, which is characteristic of the phase change that light experiences upon reflection from a high dielectric or metal surface. Using Eq. (1), the transmission for both left circularly polarized beam (LCP) and right circularly polarized beam (RCP) are obtained and shown in Figs. 2(d) and 2(e). The resonance for LCP shows much more pronounced features than that of RCP in the transmission spectra. At resonance, the dip of LCP transmission amplitude approaches almost zero (<6%, or power transmittance $|t_L|^2$ less than 0.4%), which indicates that a beam with a linear polarization transmitting through the sample would be largely converted into a RCP. Therefore, this chiral metamaterial can be used as an effective circular polarizer at the resonance frequency. The transmission phase of LCP exhibits a much larger phase modulation than that of RCP, which indicates that the refractive index for LCP changes dramatically across the resonance frequency. As shown in Fig. 3, the strong chirality observed in the terahertz metamaterial is supported by a full wave simulation using a time-domain simulation software (CST Microwave Studio^{TM}). In the simulation, the gold is described by the Drude model with plasma frequency $\omega_p = 1.37 \times 10^{16}\ \mathrm{s}^{-1}$ and scattering frequency $\gamma = 2.04 \times 10^{14}\ \mathrm{s}^{-1}$. The numerically calculated amplitudes and phases for both the transmission and reflectance agree well with the measurement results.

The electromagnetic response of the chiral metamaterials can be written as the following constituent equations:

$$\begin{pmatrix} D_x \\ D_y \end{pmatrix} = \varepsilon_0 \varepsilon \begin{pmatrix} E_x \\ E_y \end{pmatrix} + \frac{i}{c_0} \begin{pmatrix} \xi & \xi_{12} \\ -\xi_{12} & \xi \end{pmatrix} \begin{pmatrix} H_x \\ H_y \end{pmatrix},$$
$$\begin{pmatrix} B_x \\ B_y \end{pmatrix} = \frac{i}{c_0} \begin{pmatrix} -\xi & \xi_{12} \\ -\xi_{12} & -\xi \end{pmatrix} \begin{pmatrix} E_x \\ E_y \end{pmatrix} + \mu_0 \mu \begin{pmatrix} H_x \\ H_y \end{pmatrix}, \quad (2)$$

where ε and μ are the effective permittivity and permeability, ξ and ξ_{12} describe the excitation of electric (magnetic) dipoles by the magnetic (electric) field along the same and the perpendicular directions, respectively. It should be noted that the metamaterial presented here is not only chiral, but also bianisotropic due to the existence of ξ_{12}. The chiral parameter ξ lifts the degeneracy and leads to different refractive indices $n_{L/R}$ for the two circularly polarized waves, while the bianisotropic parameter ξ_{12} results in different effective impedances Z_+ and Z_- of the metamaterial for light along $+z$ (light incident from air) and $-z$ (light incident from substrate), respectively [30]. The relation $\xi_{12} = \xi \tan\theta$ holds due to the fact that the magnetic dipole and electric dipole form an angle θ in the chiral resonator [Fig. 1(b)]. ε, μ, ξ, and ξ_{12} are related to $n_{L/R}$ and $Z_{+/-}$ by

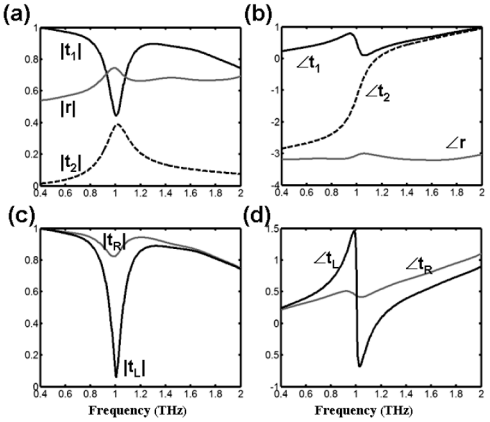

FIG. 3. The simulated transmission and reflectance of the chiral metamaterials, with the same symbol convention as in Fig. 2. (a) The amplitudes of transmission t_1 and t_2, and reflectance r. (b) The phases of t_1, t_2 and reflectance r. (c) The transmission amplitudes for left-handed and right-handed circularly polarized waves. (d) The transmission phases for left-handed and right-handed circularly polarized waves.

$$(n_{L/R} \mp \xi)^2 = \varepsilon\mu - \xi_{12}^2, \qquad Z_\pm = \frac{\mu}{\sqrt{\varepsilon\mu - \xi_{12}^2 \pm i\xi_{12}}}. \quad (3)$$

The effective parameters of the chiral metamaterial has been extracted by solving the Fresnel's equation using the measured transmission and reflectance spectra, and taking into account the substrate. The effective indices for both LCP and RCP are shown in Figs. 4(a) and 4(b). The real

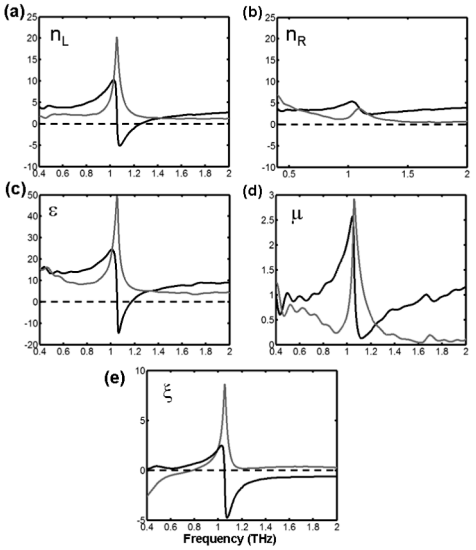

FIG. 4. Experimentally retrieved effective parameters. (a), (b) The experimentally retrieved real (black) and imaginary (gray) parts of the refractive index for left-handed and right-handed circularly polarized wave, respectively. (c)–(e) The real (black) and imaginary (gray) parts of the permittivity ε, permeability μ, and the chiral parameter ξ.

part of refractive index for the left-handed wave shows a strong modulation at the resonance frequency, and reaches negative values over the frequency range between 1.06 to 1.27 THz, with a minimum index below -5. On the other hand, the refractive index for RCP shows a much smaller modulation at the resonance frequency and remains positive over the whole frequency range. This is due to the cancellation of the resonant feature of refractive index between the contribution from the product of permittivity and permeability, and that from the chirality, as indicated by Eq. (3). Far from the resonance, the difference between the refractive indices of RCP and LCP tends to diminish, showing the significant role that the structural LC resonance plays in achieving the strong chiral behavior. The effective permittivity and permeability are extracted and shown in Figs. 4(c) and 4(d). Both of them exhibit a Lorentzian line shape. While the permittivity reaches negative values (with a minimum of -13.7) at resonance, the magnetic resonance is not strong enough to achieve negative permeability. We note that a fictitious achiral metamaterial with the same permittivity and permeability profiles would also show negative refractive index at the resonance frequency, where negative index condition $\varepsilon'\mu'' + \varepsilon''\mu' < 0$ is satisfied; however, without simultaneous negative permittivity and permeability ($\varepsilon' < 0$, $\mu' < 0$), the negative index is very weak and the overall optical properties are dominated by the imaginary part. On the other hand, as shown in Fig. 4(a), the minimum negative refractive index in the chiral metamaterial is around -5, which is quite close to the minimum value of the chiral term ξ [Fig. 4(e)]. It immediately follows that the negative refractive index has a major contribution from the chiral term.

We have demonstrated a terahertz chiral artificial material exhibiting opposite signs for the effective refractive indices of the two circularly polarized waves around the resonance frequency of 1 THz. The optical properties of the chiral metamaterials are obtained solely from the experimental measurement. The realization the chiral NIMs offers us the opportunity to explore their unique electromagnetic properties, such as negative refraction and negative reflection. The terahertz metamaterials, when combining with the optical or electrical tuning techniques [17,18,20], may lead to terahertz devices which can control the polarization of terahertz wave dynamically.

We acknowledge the help of R. Singh, T. Zentgraf, Y. M. Liu, Y. Xiong, and D. M. Wu on the characterization and simulation of the terahertz metamaterials. The UCB portion of the work was supported by AFOSR MURI (Grant No. 50432), SINAM and NSEC under Grant No. DMI-0327077. The OSU portion of the work was supported by NSF (Grant No. ECCS-0725764). We thank one referee for bringing to our notice another related work on chiral negative index metamaterials [31].

*To whom correspondence should be addressed.
xiang@berkeley.edu

[1] R. A. Shelby, D. R. Smith, and S. Schultz, Science **292**, 77 (2001).
[2] D. R. Smith *et al.*, Science **305**, 788 (2004).
[3] S. Zhang *et al.*, Phys. Rev. Lett. **94**, 037402 (2005); S. Zhang *et al.*, Phys. Rev. Lett. **95**, 137404 (2005).
[4] V. M. Shalaev *et al.*, Opt. Lett. **30**, 3356 (2005).
[5] J. B. Pendry, Phys. Rev. Lett. **85**, 3966 (2000).
[6] N. Engheta, IEEE Antennas Wireless Propag. Lett. **1**, 10 (2002).
[7] K. L. Tsakmakidis *et al.*, Nature (London) **450**, 397 (2007).
[8] S. Tretyakov *et al.*, J. Electromagn. Waves. Appl. **17**, 695 (2003).
[9] J. B. Pendry, Science **306**, 1353 (2004).
[10] C. Monzon and D. W. Forester, Phys. Rev. Lett. **95**, 123904 (2005).
[11] S. Tretyakov, A. Sihvola, and A. Jylha, Photonics Nanostruct. Fundam. Appl. **3**, 107 (2005).
[12] Q. Cheng *et al.*, Opt. Commun. **276**, 317 (2007).
[13] C. Zhang and T. J. Cui, Appl. Phys. Lett. **91**, 194101 (2007).
[14] X. C. Zhang, Phys. Med. Biol. **47**, 3667 (2002).
[15] T. J. Yen *et al.*, Science **303**, 1494 (2004).
[16] C. R. Williams, Nat. Photon. **2**, 175 (2008).
[17] W. J. Padilla *et al.*, Phys. Rev. Lett. **96**, 107401 (2006).
[18] H. T. Chen *et al.*, Nature (London) **444**, 597 (2006).
[19] A. K. Azad *et al.*, Opt. Lett. **31**, 634 (2006).
[20] H. T. Chen *et al.*, Nat. Photon. **2**, 295 (2008).
[21] A. V. Rogacheva *et al.*, Phys. Rev. Lett. **97**, 177401 (2006).
[22] E. Plum *et al.*, Appl. Phys. Lett. **90**, 223113 (2007).
[23] M. Decker *et al.*, Opt. Lett. **32**, 856 (2007).
[24] N. Kanda *et al.*, Opt. Express **15**, 11117 (2007).
[25] S. Linden *et al.*, Science **306**, 1351 (2004).
[26] D. Grischkowsky *et al.*, J. Opt. Soc. Am. B **7**, 2006 (1990).
[27] X. C. Lu *et al.*, Appl. Phys. Lett. **92**, 121103 (2008).
[28] A. K. Azad, Y. Zhao, and W. Zhang, Appl. Phys. Lett. **86**, 141102 (2005); J. Han *et al.*, Appl. Phys. Lett. **91**, 071122 (2007).
[29] D. Grischkowsky and S. Keiding, Appl. Phys. Lett. **57**, 1055 (1990).
[30] M. S. Rill *et al.*, Nature Mater. **7**, 543 (2008).
[31] E. Plum *et al.*, arXiv:0806.0823.